Electric-field-controlled ferromagnetism in high-Curie-temperature $Mn_{0.05}Ge_{0.95}$ quantum dots

Faxian Xiu[1]*, Yong Wang[2]*, Jiyoung Kim[1], Augustin Hong[1], Jianshi Tang[1], Ajey P. Jacob[3], Jin Zou[2] and Kang L. Wang[1]†

Electric-field manipulation of ferromagnetism has the potential for developing a new generation of electric devices to resolve the power consumption and variability issues in today's microelectronics industry. Among various dilute magnetic semiconductors (DMSs), group IV elements such as Si and Ge are the ideal material candidates because of their excellent compatibility with the conventional complementary metal–oxide–semiconductor (MOS) technology. Here we report, for the first time, the successful synthesis of self-assembled dilute magnetic $Mn_{0.05}Ge_{0.95}$ quantum dots with ferromagnetic order above room temperature, and the demonstration of electric-field control of ferromagnetism in MOS ferromagnetic capacitors up to 100 K. We found that by applying electric fields to a MOS gate structure, the ferromagnetism of the channel layer can be effectively modulated through the change of hole concentration inside the quantum dots. Our results are fundamentally important in the understanding and to the realization of high-efficiency Ge-based spin field-effect transistors.

The control of magnetic properties has traditionally been accomplished by applying electric currents. Unfortunately, using currents poses significant challenges in reducing power consumption and in realizing device miniaturization. In contrast, electric-field control of ferromagnetism in a DMS system offers potential advantages in device functionality and power dissipation[1]. It promises a new breed of magneto-electronic devices to extend the scaling of microelectronics to the next generation of nanometre-sized integrated chips for low power consumption and low variability[2]. To understand and exploit this controllability, several theoretical models were proposed to explain ferromagnetic coupling in DMSs on a microscopic scale, including Zener's kinetic-exchange[3,4], double-exchange[5] and the Ruderman–Kittel–Kasuya–Yosida interaction[6,7]. These models share a common feature: spontaneous ferromagnetic order is carrier-mediated through an increase in carrier concentration. Although the precise theories to explain this phenomenon are still under debate[3,6,8], this effect has been experimentally observed in group III–V materials such as (In, Mn)As and (Ga, Mn)As DMSs (refs 9–11). Electric-field-controlled ferromagnetism has also been successfully demonstrated in III–V materials on the basis of the carrier-mediated effect in gated MOS and p–n junction devices[9,10,12,13]. As the study of III–V DMSs continues, the quest for practical spintronic devices working at ambient temperature calls for a new material candidate with a high Curie temperature ($T_C > 300$ K), controllable ferromagnetism and easy integration with complementary MOS platforms[3,14].

In recent years, Mn-doped Ge DMS has attracted extensive attention because of its compatibility with today's Si microelectronics and the possibility to have higher Curie temperatures than those of group III–V materials[15–19]. In particular, MnGe nanostructures such as quantum dots may offer unique and salient physical properties arising from size and quantum confinement effects, affecting carrier transport, spin lifetimes and interactions of spins, and thus ferromagnetic properties[20]. With this motivation, we had previously investigated the magnetic properties of Mn_xGe_{1-x} nanostructures by ion implantation of Mn (ref. 21). We demonstrated the hole-mediated effect in Mn_xGe_{1-x} nanostructures and the modulation of their ferromagnetism by applying gate biases in MOS capacitors at a low temperature of 10 K. However, metallic precipitates such as Mn_5Ge_3 and $Mn_{11}Ge_8$ and implantation damage were found in these nanostructures, which made the system rather complex and might have partly jeopardized the hole-mediated effect. In the present research, we demonstrate successful development of high-T_C self-assembled $Mn_{0.05}Ge_{0.95}$ quantum dots by molecular-beam epitaxy (MBE). The structural and magnetic characterizations confirm the formation of single-crystalline DMS quantum dots without observable Mn_5Ge_3 or $Mn_{11}Ge_8$ precipitates. The T_C of the material was measured by a superconducting quantum interference device (SQUID) magnetometer and obtained using Arrott plots, showing T_C above 400 K. By using a similar MOS device structure as illustrated in ref. 21, the effective manipulation of ferromagnetism of these quantum dots was clearly observed at 100 K. The realization of high-T_C $Mn_{0.05}Ge_{0.95}$ DMS quantum dots sets the stage for room-temperature spin field-effect transistor devices, although the electric-field effect is shown only up to 100 K because of leakage currents in our MOS capacitors.

Structural characteristics of $Mn_{0.05}Ge_{0.95}$ quantum dots

Cross-section transmission electron microscopy (TEM) was carried out to determine the structural characteristics and the Mn composition of the $Mn_{0.05}Ge_{0.95}$ quantum dots. High-resolution TEM (HRTEM) reveals that a quantum dot has a dome shape with a base diameter of about 30 nm and a height of about 8 nm (Fig. 1a,d). The interface between the dot and the Si substrate has

[1]Device Research Laboratory, Department of Electrical Engineering, University of California, Los Angeles, California 90095, USA, [2]Materials Engineering and Centre for Microscopy and Microanalysis, University of Queensland, Brisbane, Queensland 4072, Australia, [3]Intel Corporation, Santa Clara, California 95054, USA. *These authors contributed equally to this work. †e-mail: wang@ee.ucla.edu.

337
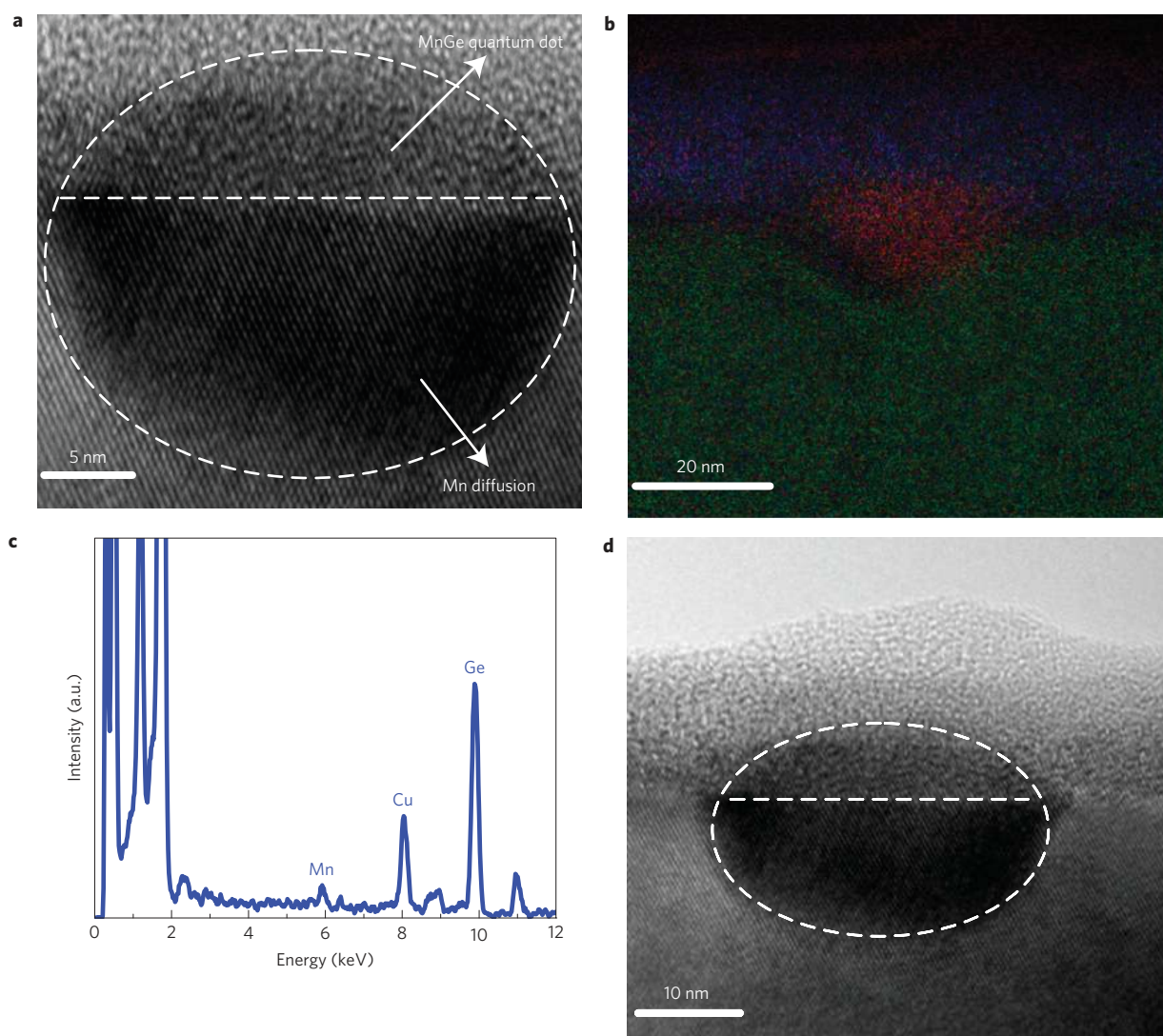
Figure 1 | Structural properties of Mn$_{0.05}$Ge$_{0.95}$ quantum dots grown on a p-type Si substrate. a, A HRTEM cross-section image of a typical Mn$_{0.05}$Ge$_{0.95}$ quantum dot showing the detailed lattice structure. The size of this Mn$_{0.05}$Ge$_{0.95}$ quantum dot is about 30 nm in base diameter and 8 nm in height. Note that Mn also diffuses into the Si substrate, which is shown directly underneath the Mn$_{0.05}$Ge$_{0.95}$ quantum dot. The interface is coherent and no pronounced defects are observed. **b**, EELS composition mapping of the Mn distribution (reddish points). Mn was found to distribute uniformly in the Mn$_{0.05}$Ge$_{0.95}$ quantum dot and the Mn-diffused Si area. **c**, Typical EDS spectrum showing that both Mn and Ge are present in the Mn$_{0.05}$Ge$_{0.95}$ quantum dot. The average Mn concentration in the quantum dots was estimated to be 4.8 ± 0.5%. **d**, An HRTEM image showing the surrounding area.

excellent lattice coherence. A careful inspection reveals that the dot is single crystalline, without evidence of pronounced dislocations or stacking faults. However, because of the heavy Mn doping, it is possible that some amount of point defects (such as Mn interstitials) may be present inside the dot, which is beyond the detection capability of conventional TEM. It is noted that Mn-doped single-crystalline (In$_{0.84}$Mn$_{0.16}$)As quantum dots were also found to maintain nearly perfect crystallinity, although the Mn doping exceeded the solubility limit in InAs (refs 22, 23).

Directly underneath the Mn$_{0.05}$Ge$_{0.95}$ quantum dot, Mn diffuses into the Si substrate and forms a strained MnSi area, which has the same diameter as the top Mn$_{0.05}$Ge$_{0.95}$ quantum dot, but a height of about 16 nm (Fig. 1a,d). This diffusion behaviour is not unusual, as it was also observed in (In, Mn)As and (In, Cr)As quantum-dot systems[24,25]. However, the migrations of Mn into the substrate make it difficult to accurately determine the Mn concentration inside the dot. To address this challenge, we have carried out both extensive electron energy-loss spectroscopy (EELS) and energy dispersive X-ray spectroscopy (EDS) experiments (in scanning TEM mode) to

analyse the Mn composition at the nanoscale. As shown in Fig. 1b, the discrete reddish dots representing Mn dopants distributed uniformly in the MnGe quantum dot and the Mn diffusion area, suggesting that the Mn concentrations in both regions are nearly identical. Extensive EELS and EDS studies further confirmed the presence of Mn and Ge in the MnGe quantum dots (Fig. 1b,c). It should be mentioned that when the EDS was carried out, electron probes of several nanometres in diameter were illuminated on the Mn$_{0.05}$Ge$_{0.95}$ quantum dots and their underlying Si substrate. Consequently, Si peaks are constantly observed in the EDS spectra. To estimate the Mn concentrations, we carried out a quantitative analysis of the atomic percentages of Mn and Ge and artificially discounted the Si peak. The EDS analysis over many quantum dots reveals a Mn/Ge atomic ratio of about 0.144:1. As approximately 1/3 volume fraction of Mn is distributed in the MnGe quantum dot, as shown in Fig. 1a,b, the average Mn concentration can be estimated to be 4.8 ± 0.5%. Note that the deviation was determined by a thorough study of many MnGe quantum dots. Both the HRTEM investigations and the composition analysis suggest that each
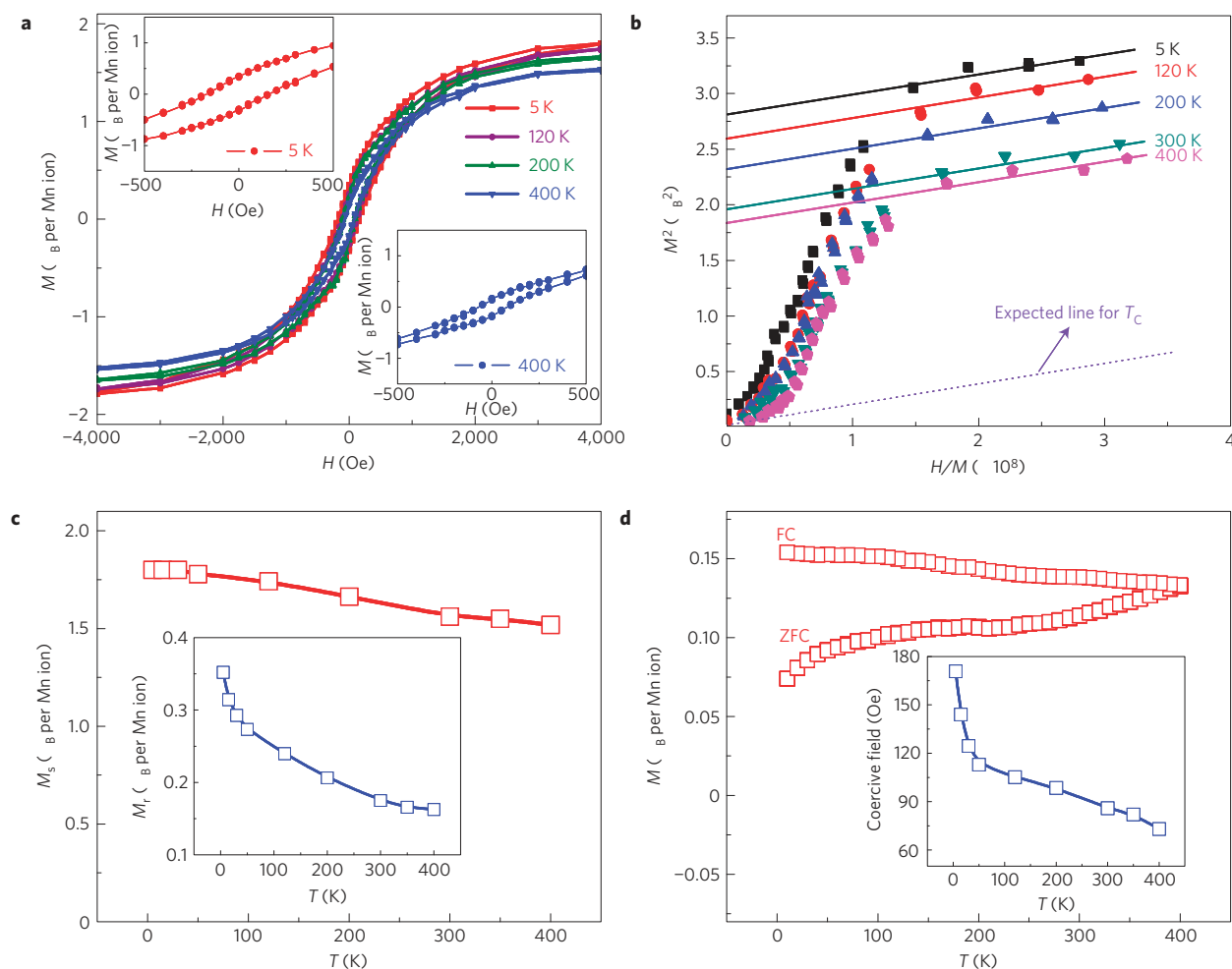
Figure 2 | Magnetic properties of Mn$_{0.05}$Ge$_{0.95}$ quantum dots grown on a p-type Si substrate. a, Hysteresis loops measured at different temperatures from 5 to 400 K. The observation of a hysteresis loop at 400 K indicates strong ferromagnetism above room temperature. Insets: Hysteresis loops at 5 and 400 K. **b**, The Arrott plots were used to obtain T_C. Consistent with **a**, the T_C is projected to be above 400 K. **c**, The temperature dependence of saturation moments. Inset: The remnant moments with respect to temperature. **d**, Zero-field-cooled (ZFC) and field-cooled (FC) magnetization of quantum dots with a magnetic field of 100 Oe. Inset: Coercivity values at different temperatures. The external magnetic field is in parallel with the sample surface.

individual quantum dot is a single-crystalline DMS system. More TEM observations are also available in Supplementary Fig. S1.

Magnetic properties of Mn$_{0.05}$Ge$_{0.95}$ quantum dots

Figure 2a and its insets show the temperature-dependent hysteresis loops when the external magnetic field is parallel to the sample surface (in-plane). The field-dependent magnetization indicates a strong ferromagnetism above 400 K. The saturation magnetic moment per Mn atom is roughly estimated to be 1.8 μ_B at 5 K. Note that this value could have a large error because it is extremely difficult to precisely calculate the total volume of quantum dots, as they have a distribution of volumes. Nevertheless, a fraction of roughly 60% of the Mn is estimated to be activated assuming that each Mn has a moment of 3 μ_B (refs 16, 26–28). Arrott plots (see the Methods section) were also used to evaluate the T_C (refs 19, 29), as shown in Fig. 2b. We observe that even at 400 K, the intercept $1/\chi$ (χ is susceptibility) on the H/M axis does not vanish, which means that χ still has a finite value and the T_C has not been reached yet. By using the slope obtained at 400 K, a dashed line can be drawn, as shown in Fig. 2b, in which the T_C is projected to be beyond 400 K. This is in good agreement with the data from the hysteresis loops showing magnetic order above 400 K. Figure 2c and its inset show the temperature-dependent saturation and remnant moments per Mn ion, respectively. Both

of them demonstrate weak temperature dependencies and a substantial amount of magnetization moment remains even at 400 K. This phenomenon has also been observed recently in several nanostructure systems[22,25,30,31]. For example, 1% of Mn doping in Ge nanowires produces room-temperature ferromagnetism and a weak temperature dependence of the saturation moments[30,31]; Cr-doped InAs DMS quantum dots with a Cr/In flux ratio between 0.026 and 0.18 show a T_C beyond 400 K and the remnant moment remains almost the same in the temperature range from 5 to 300 K (ref. 25). With a Mn concentration of 16% in InAs quantum dots, the temperature-dependent magnetization remains nearly constant until it reaches 400 K (but no electric-field dependence of magnetization was reported)[22]. In contrast, the highest T_C for III–V DMS bulk materials achieved so far is 185 K (ref. 32). Whereas the discrepancy in the Curie temperatures is still under investigation, the enhanced ferromagnetism in these nanostructures may be attributed to quantum confinement effects[22].

Zero-field-cooled and field-cooled magnetizations were measured with a magnetic field of 100 Oe, as shown in Fig. 2d. The magnetic moments do not drop to zero, suggesting a high T_C beyond 400 K, which is in good agreement with the Arrott plots in Fig. 2b. From these two curves, one can also infer the formation of a single phase in this material system, that is, DMS quantum dots, which is surprisingly similar to the high-T_C DMS Mn$_{0.05}$Ge$_{0.95}$ nanowires[33].
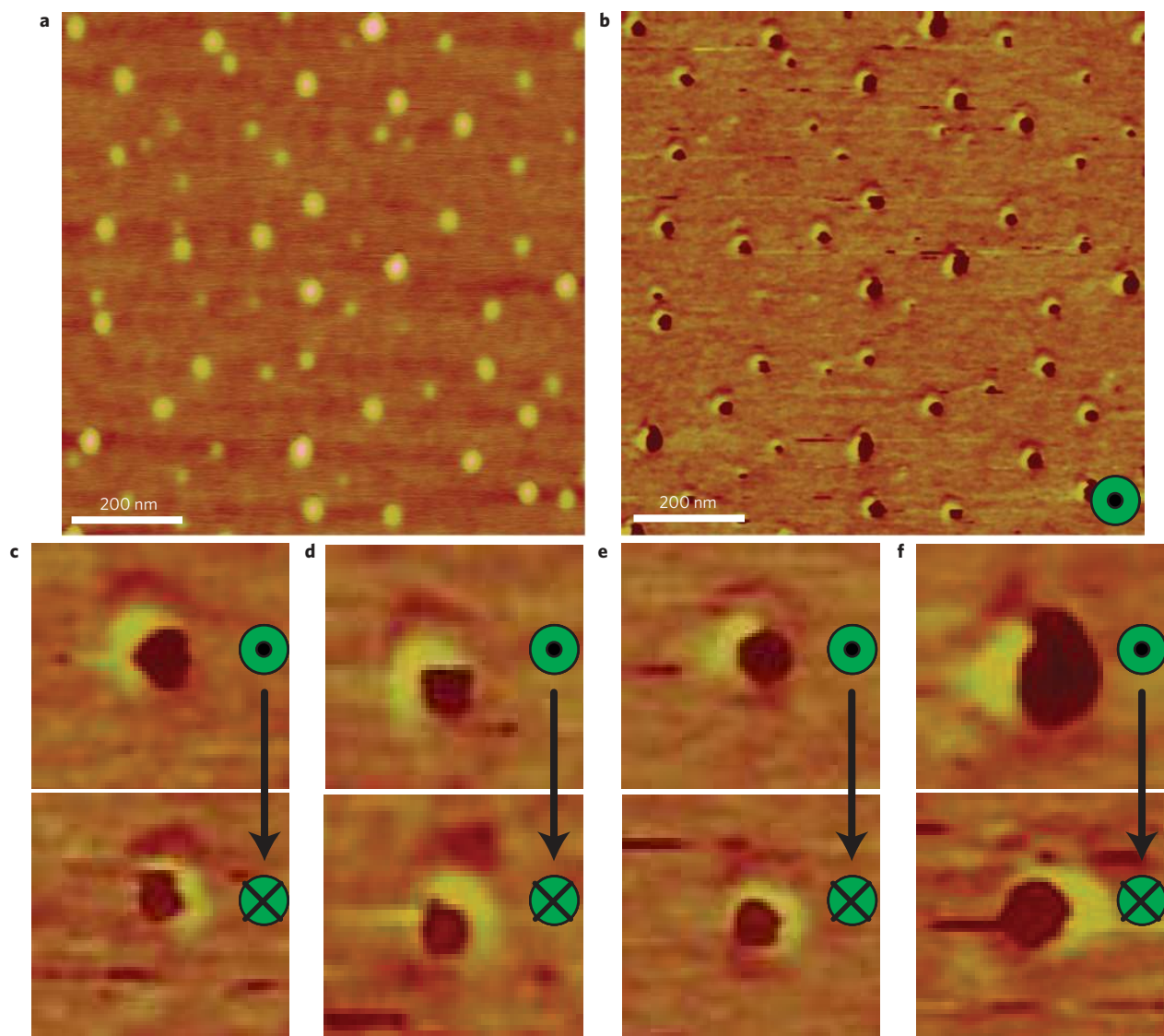
Figure 3 | AFM and MFM images of $Mn_{0.05}Ge_{0.95}$ quantum dots measured at 320 K. a, Typical AFM image of $Mn_{0.05}Ge_{0.95}$ quantum dots.
b, Corresponding MFM image with the tip magnetization pointing towards the sample. **c–f**, Magnified MFM images of individual quantum dots taken from **b**. From these MFM measurements, opposite contrast was observed when applying opposite magnetization to the tip. The results suggest that the magnetic signals come from the $Mn_{0.05}Ge_{0.95}$ quantum dots. The formation of Mn_5Ge_3 and $Mn_{11}Ge_8$ can be excluded because of their low T_C values of 296–300 K.

The wide separation of the zero-field-cooled and field-cooled curves in the temperature range of 5–400 K shows the irreversibility of susceptibilities, possibly arising from strain-induced anisotropy because a large lattice mismatch exists between Si and Ge (ref. 34). The temperature-dependent coercivity is shown in the inset of Fig. 2d. Similarly to Mn_xGe_{1-x} nanowires[31], the coercivity decreases from 170 Oe (at 5 K) to 73 Oe (at 400 K). The small coercivity in the entire temperature range measured features a soft ferromagnetism that originates from Mn ions diluted in the Ge matrix[35]. The above magnetic properties support the fact that the $Mn_{0.05}Ge_{0.95}$ quantum dots show a DMS-type ferromagnetic order.

It is well known that the direct interaction (superexchange) between the d-shells of the adjacent Mn atoms leads to an antiferromagnetic configuration of the d-shell spins[36]. Therefore, the presence of Mn–Mn clusters would lead to antiferromagnetism; however, when this pair is surrounded by other Mn atoms, ferri- or ferromagnetic coupling may appear. However, our extensive HRTEM experiments did not reveal observable Mn clusters, although such a possibility cannot be completely excluded

(Fig. 1 and Supplementary Fig. S1). Thus, the origin of the strong ferromagnetism in our case possibly comes from the $Mn_{0.05}Ge_{0.95}$ quantum dots as a result of the hole mediation process. In general, when Mn dopants are introduced into Ge, they produce two acceptor levels, that is, 0.16 and 0.37 eV above the valence band[37]. When the doping concentration becomes high, the impurity bands can develop (instead of being separate acceptor levels). However, theoretically the formation of such impurity bands may not affect the physics of ferromagnetism[38]. In the following, we will analyse the Mn-doping behaviour by considering a single acceptor level of 0.16 eV in an approximate form. At a sufficiently high temperature, Mn acceptors can be activated to generate holes. These holes are itinerant among a number of Mn ions and align Mn local spins along one direction through the p–d exchange coupling to reduce the total energy of the system, resulting in hole-mediated ferromagnetism[39,40]. Experimentally this phenomenon has been widely observed in several material systems, such as group III–V (GaAs and InAs; refs 9, 41), group II–VI (ZnO; ref. 42) and group IV (Ge; ref. 21) materials. Although most research focuses
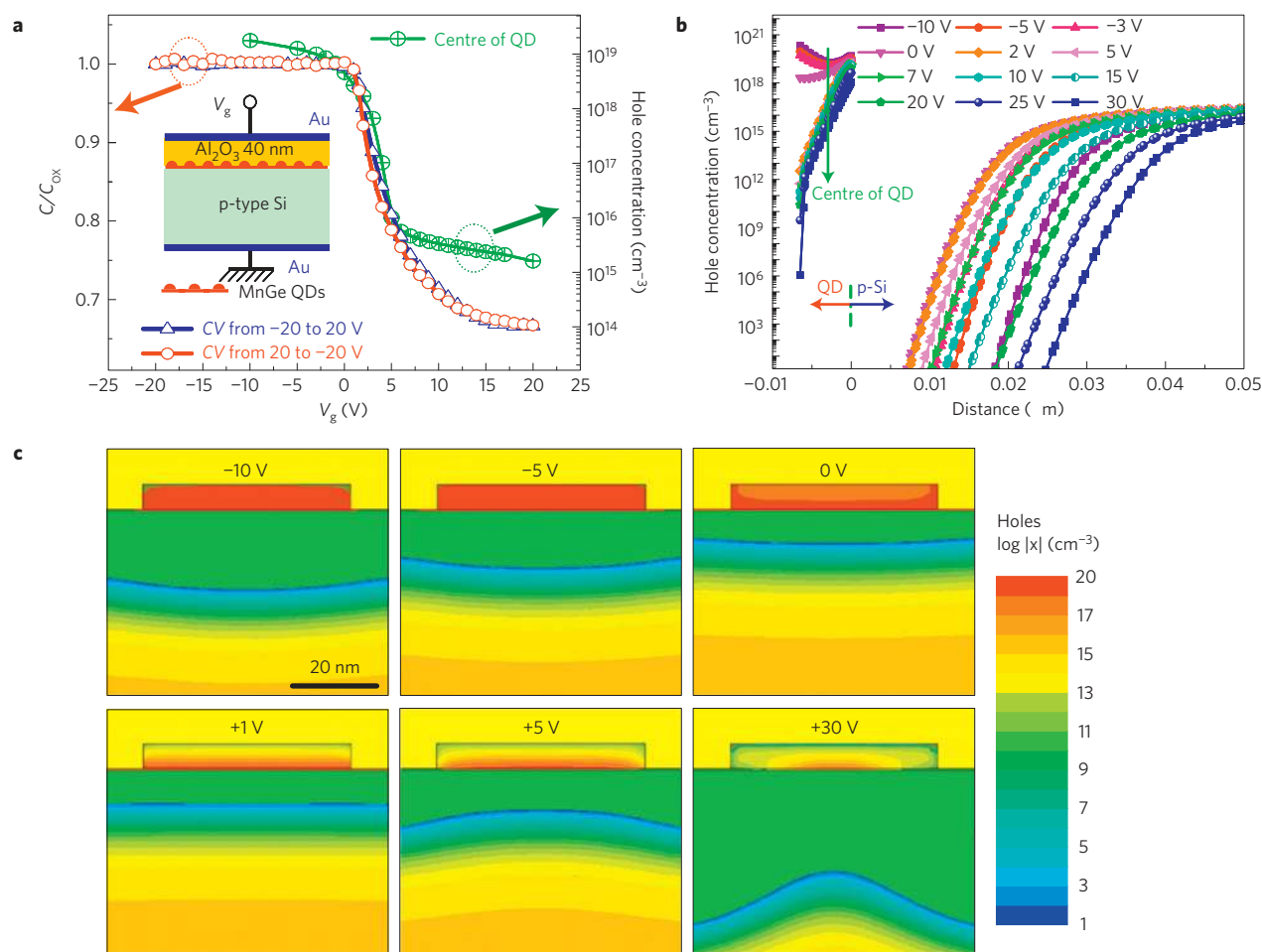
Figure 4 | Characterization and simulation of a MOS device using Mn$_{0.05}$Ge$_{0.95}$ quantum dots as the channel layer. a, C–V curves measured at 77 K with a frequency of 100 kHz. The forward and backward scans are plotted in blue and red, respectively. The plot clearly shows a transition between hole accumulation at negative bias and hole depletion at positive bias. The green curve shows the simulated hole concentrations as a function of the gate bias at the centre of the Mn$_{0.05}$Ge$_{0.95}$ quantum dot (QD). Inset: Schematic of the device. **b**, Simulated hole concentrations in the Mn$_{0.05}$Ge$_{0.95}$ quantum dot with different biases. **c**, Maps of hole concentration under different gate voltages at 77 K.

on bulk DMSs, it is of particular interest to study the origin of ferromagnetism in quantum structures. Previously, we and others have suggested that the carrier confinement in a DMS quantum dot can strengthen hole localization and subsequently enhance the thermal stability of magnetic polarons, giving rise to a higher T_C than those of bulk films[21,24]. Similarly, the quantum-confined holes could hybridize with the localized spins of Mn^{2+} through the well-known p–d exchange coupling to induce the ferromagnetism[43]. Nevertheless, all of the arguments above suggest that when it comes to nanoscale structures, such as quantum dots and nanowires, the quantum confinement effect comes into being, which significantly influences the exchange coupling between the confined holes and the localized Mn^{2+}. However, the detailed theoretical treatise is still not available at this stage.

Besides the Mn-doping effect, we also take advantage of the quantum confinement effect between p-type Si and p-type Mn$_{0.05}$Ge$_{0.95}$, which provides sufficient holes to induce the hole-mediated effect. It is well established that the heterostructure between p-type Si and p-type Ge has a valence-band offset, in which the holes can be trapped and form a two-dimensional hole gas in the interface (see the band diagram in Supplementary Fig. S2; refs 37, 44). The persistent ferromagnetism at high temperature could be attributed to the enhanced hole-mediated effect arising from the formation of the two-dimensional hole gas in between Si and the Mn$_{0.05}$Ge$_{0.95}$ quantum dots. However, as mentioned above,

we cannot completely exclude the possibility of defect formation and Mn aggregation resulting from the Mn doping, which may also enhance the T_C (refs 45–47).

Atomic force microscopy (AFM) and magnetic force microscopy (MFM) measurements were carried out to investigate the morphology and ferromagnetism of the Mn$_{0.05}$Ge$_{0.95}$ quantum dots at 320 K, respectively. The average dot size is about 50 nm in base diameter and 6 nm in height. The dot density is about 6×10^9 cm^{-2} (Fig. 3a). The corresponding MFM image was taken by lifting the MFM probe 25 nm above the topographic height of the sample in phase detection mode (Fig. 3b). The appearance of bright and dark areas in the MFM image clearly shows the formation of magnetic domains in the Mn$_{0.05}$Ge$_{0.95}$ quantum dots, which is similar to (In, Mn)As DMS quantum dots[22]. Figure 3c–f shows magnified MFM images of several individual Mn$_{0.05}$Ge$_{0.95}$ quantum dots. By reversing the tip magnetization, opposite contrast was observed for each dot, indicating that the magnetic signals originated from the top Mn$_{0.05}$Ge$_{0.95}$ quantum dots. Note that each quantum dot is a single-domain 'particle'. During the magnetization process, the domain would rotate preferentially along the magnetic field to produce net magnetization moments. As the experiments were carried out at 320 K, the formation of metallic phases such as Mn$_5$Ge$_3$ and Mn$_{11}$Ge$_8$ can be easily ruled out, because they have low Curie temperatures of 296–300 K (ref. 48). Overall, the above MFM results agree well with the TEM observations
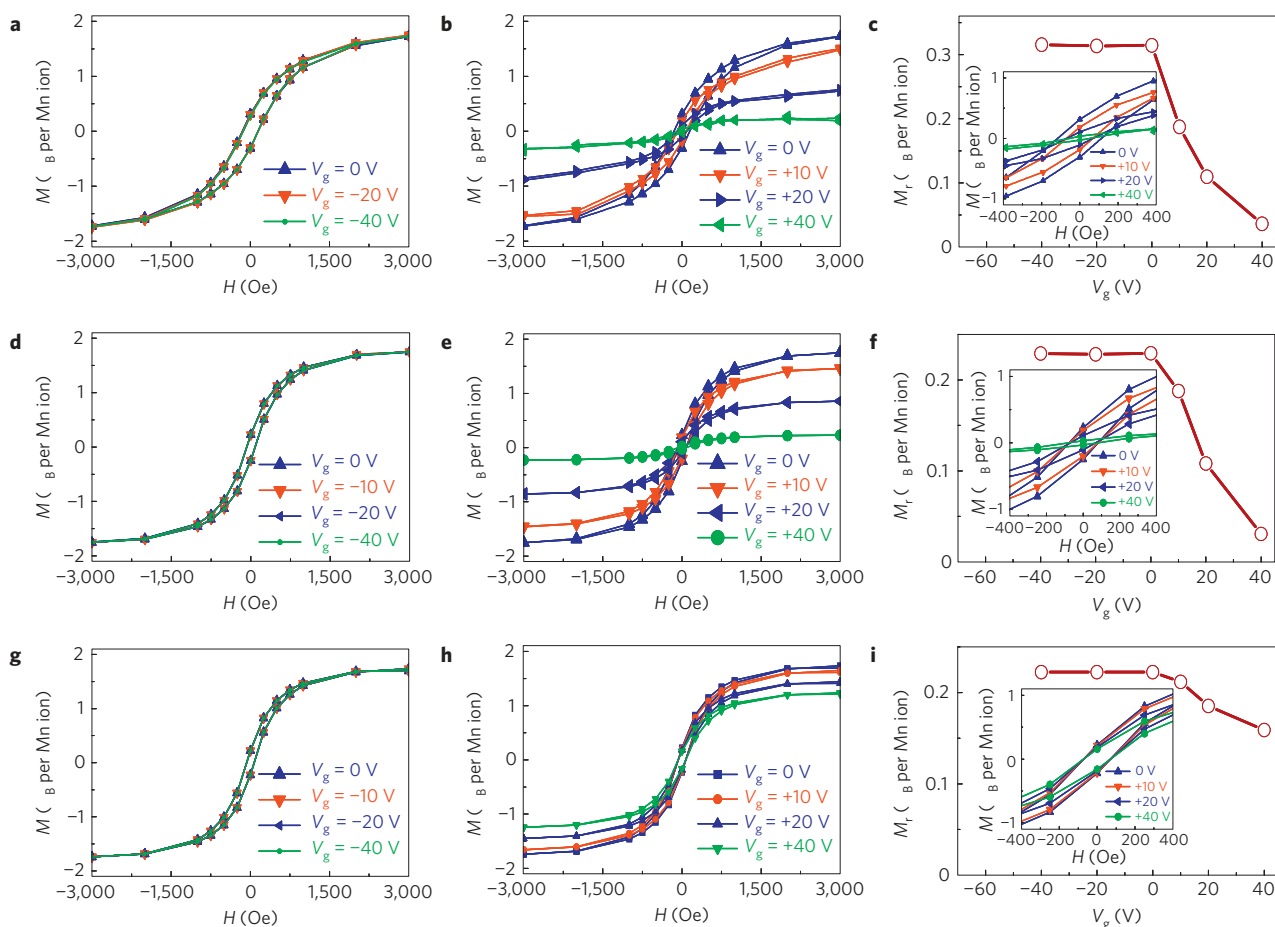
Figure 5 | Electric-field-controlled ferromagnetism. a–i, Control of ferromagnetism of $Mn_{0.05}Ge_{0.95}$ quantum dots by applying electric field at 50 K (**a–c**), 77 K (**d–f**) and 100 K (**g–i**). **a,d** and **g** show the hysteresis loops with zero and negative bias of −10, −20 and −40 V on the gate. **b,e** and **h** show the hysteresis loops with zero and positive bias of +10, +20 and +40 V. **c,f** and **i** show the remnant moments with respect to the gate bias. The insets to **c**, **f** and **i** are magnified views from the central part of **b**, **e** and **h** to clearly show the change of remnant moments, respectively. It is found that both the saturation and remnant moments can be manipulated by applying biases on the MOS gate at 50, 77 and 100 K.

and the ferromagnetic order at high temperature obtained in the SQUID measurements.

MOS device characterizations and simulations

A MOS device was fabricated to study the modulation of ferromagnetism in the $Mn_{0.05}Ge_{0.95}$ quantum dots by electric field. The inset of Fig. 4a shows the device structure, consisting of a metal gate (Au, 200 nm), Al_2O_3 (40 nm), $Mn_{0.05}Ge_{0.95}$ quantum dots (6 nm), a wetting layer (<0.6 nm), a p-type Si substrate ($1 \times 10^{18} cm^{-3}$) and a back metal contact (Au, 200 nm). Capacitance–voltage ($C-V$) curves were measured at 77 K with a frequency of 100 kHz. Voltage traces were recorded in two directions and the small difference between the forward and backward scans indicated the presence of a small amount of trapped charges at the Al_2O_3 and/or the interface (Fig. 4a, blue and red curves; ref. 37). By increasing the gate voltage from negative to positive values, the $Mn_{0.05}Ge_{0.95}$ quantum dots can accumulate holes (accumulation mode), then deplete holes (depletion mode) and finally fill with electrons on top of the quantum dot (inversion mode). It is noted that at zero bias, the device is already at the accumulation mode (with holes) in the $Mn_{0.05}Ge_{0.95}$ quantum dots. The accumulation of holes can be explained by the quantum confinement effect resulting from the valence-band offset between Si and Ge (see Supplementary Fig. S2; ref. 44).

To estimate the distributions of holes with different gate biases, we have carried out systematic simulations using the MEDICI

software[49]. Figure 4b shows the dependencies of the calculated hole concentrations on gate voltage at 77 K. At zero bias, because of the quantum confinement effect, the hole concentrations reach 2.1×10^{18} and $4.4 \times 10^{18} cm^{-3}$ for the top and centre of the $Mn_{0.05}Ge_{0.95}$ quantum dot, respectively (see also Supplementary Fig. S2). By applying a negative bias, holes start to accumulate in the $Mn_{0.05}Ge_{0.95}$ quantum dot and the hole concentration increases. For instance, at −10 V, the hole concentration increases about 50 times on the top and four times in the centre of the quantum dot, as calculated from Fig. 4b (Supplementary Fig. S2). The depletion width in the proximity of the interface remains almost the same under the negative biases (−10–0 V). However, by applying a positive voltage, the holes are depleted into the p-type Si substrate. The hole concentration changes markedly at the top part of the $Mn_{0.05}Ge_{0.95}$ quantum dot (10^{11}–$10^{13} cm^{-3}$), and at the centre part, a concentration of 10^{14}–$10^{16} cm^{-3}$ remains in the voltage range of +1–30 V (at 77 K, Supplementary Fig. S2). The depletion width also changes noticeably from 7 nm (purple down-triangle for 0 V) to 25 nm (dark blue square for +30 V), as shown in Fig. 4b. The simulated hole concentrations at the centre of the quantum dot are plotted as a function of gate bias at 77 K in Fig. 4a (green curve). Figure 4c illustrates a general hole density redistribution map in a logarithmic scale. It can be seen that the hole concentration in the $Mn_{0.05}Ge_{0.95}$ quantum dot decreases as the bias increases from −10 to +30 V; this result further confirms the hole accumulation, depletion and

inversion processes as shown in the $C-V$ measurements (Fig. 4a, blue and red curves).

Electric-field-controlled ferromagnetism

In our previous study, we have reported the formation of DMS Mn_xGe_{1-x} nanostructures in Ge substrate by using Mn ion implantation through a nanodot mask[21]. Although Mn clusters and metallic phases were observed, it was the first demonstration of the control of ferromagnetic order by an electrically biased MOS device using Mn_xGe_{1-x} as the channel material. In the present research, the channel material of $Mn_{0.05}Ge_{0.95}$ self-assembled DMS quantum dots is confirmed to lack metallic phases (Mn_5Ge_3 and $Mn_{11}Ge_8$). In addition, the ferromagnetic order was observed at above 400 K, which shows potential applications for spin electronic devices operating at room temperature and above.

Figure 5 shows the electric-field-controlled ferromagnetism at 50 K (Fig. 5a–c), 77 K (Fig. 5d–f) and 100 K (Fig. 5g–i). Owing to the similarity of the data, we take the case of 77 K as an example to describe the device operation in Fig. 5d–f. Figure 5d and e show the hysteresis loops measured by a SQUID magnetometer with negative and positive biases on the MOS gate at 77 K, respectively. Under a negative bias, the holes are attracted into the channel of the device (accumulation). In this circumstance, however, the hysteresis loop does not show a remarkable change (Fig. 5d). This could be explained by the fact that even at 0 V, the quantum-dot device has already accumulated enough holes to induce ferromagnetism. In other words, the hole-mediated effect is sufficient to align most of the activated Mn ions along one direction in each individual quantum dot. Further increasing the negative bias does not significantly increase the hole concentration. On the contrary, with positive bias, a large amount of holes are depleted into the p-type Si, so that the hole-mediated effect is notably reduced. In fact, the surface of the device can have a high concentration of electrons if the leakage is limited (inversion). As a result, the Mn ions start to misalign because of the lack of holes. The saturation moment per Mn ion decreases more than ten times as the gate bias increases from 0 to +40 V (Fig. 5e). It should be noted that, at +40 V, the saturation and remnant moments of the $Mn_{0.05}Ge_{0.95}$ quantum dots become fairly weak, resembling a 'paramagnetic-like' state. From the device simulations, it is shown that at a large positive bias, the holes are significantly depleted into the Si substrate (Supplementary Fig. S2), leading to reduced ferromagnetism. Figure 5f summarizes the change of the remnant moments as a function of gate voltage. A similar trend in the carrier density as a function of the gate bias was observed from $C-V$ curves, suggesting a strong correlation between the hole concentrations and ferromagnetism, that is, the hole-mediated effect. The inset in Fig. 5f shows a magnified picture to clearly show the change of remnant moments with respect to the gate bias. By increasing the measurement temperature to 100 K (Fig. 5g–i), the modulation of the ferromagnetism becomes less pronounced compared with those at 50 and 77 K owing to the increased leakage current in our MOS devices (Supplementary Fig. S3). The above results evidently demonstrate that the hole-mediated effect does exist in this material system, which is also supported by our previous experiments[21]. The discovery of high-T_C MnGe DMS quantum dots and electric-field-controlled ferromagnetism paves the way towards practical spintronic devices operable at room temperature.

Methods

Growth. $Mn_{0.05}Ge_{0.95}$ quantum dots were grown in a Perkin-Elmer solid-source MBE system. High-purity Ge (99.9999%) and Mn (99.99%) sources were evaporated from conventional high-temperature effusion cells. Before the growth, Si substrates were cleaned by H_2SO_4:H_2O_2 = 5:3 and 1% HF for 1 min at each step. This process was repeated three times with a final step of HF etching. The remaining native oxide was removed by annealing the silicon substrates at 850 °C inside the MBE chamber for 10 min with a base pressure of 10^{-10} torr. Then,

self-assembled $Mn_{0.05}Ge_{0.95}$ DMS quantum dots were deposited at 450 °C with a Ge growth rate of 0.2 Å s^{-1} and an adjustable Mn flux as the dopant source. The nominal thickness was designed to be 1.2 nm.

The Arrott plots. A SQUID (Quantum Design) was used to measure the field- and temperature-dependent magnetization. The diamagnetic contribution of the Si substrate was subtracted from all of the measurements. The Arrott plots were used to evaluate the T_C (Fig. 2b; refs 19, 29). By neglecting the high-order terms, the magnetic field can be expressed as[50],

$$H = \frac{1}{\chi}M + \beta M^3 \quad \text{or} \quad \frac{H}{M} = \frac{1}{\chi} + \beta M^2 \quad (1)$$

where H is the external magnetic field, M is the magnetic moment from the sample, χ is the susceptibility and β is a materials-dependent constant. According to equation (1), M^2 can be plotted as a function of H/M. When H/M is extrapolated to $M^2 = 0$, the intercept on the H/M axis gives $1/\chi$. The T_C for this material can be obtained when $1/\chi$ vanishes.

MEDICI simulations. The simulated device model was constructed by considering the experimental conditions. The quantum dots were represented by a rectangle with a width of 50 nm, a height of 6 nm and a spacing of 150 nm (Supplementary Fig. S2). Mn has two acceptor levels in Ge, providing holes. In the MEDICI simulations, only one level ($E_a = 0.16$ eV) was considered because another deeper acceptor level ($E_a = 0.37$ eV) could barely contribute to the hole concentration. We also assumed that 60% of the Mn atoms were activated in the modelling (according to the experimental data). As the simulations did not consider the formation of the impurity bands and the compensation effects that occur in the real experiments, the calculated hole concentrations could be inaccurate. This is the limitation of our calculations. However, the underlying physics of the field-controlled ferromagnetism would not change because the $C-V$ measurements clearly revealed a carrier redistribution process in Fig. 4a. On the other hand, it is noted that the calculated hole concentration varies over four orders of magnitude when comparing $V_g = -10$ V with $V_g = +20$ V (see Fig. 4b and Supplementary Fig. S2). Thus, the neglected compensation effect is unlikely to affect the quality of the carrier redistribution process, and the errors in the estimated hole concentrations would not change the general shape of the $C-V$ curve. During the MEDICI simulations, several physical models were also considered for more accurate calculations, including the freeze-out effect at low temperature, the Fermi–Dirac model for carrier occupations and quantum mechanical corrections by invoking Philips's bandgap-widening effect[49].

Device fabrication and characterizations. The MOS capacitors were first made by depositing 40-nm-thick Al_2O_3 on top of the $Mn_{0.05}Ge_{0.95}$ quantum-dot layer at 250 °C through an atomic layer deposition technique. The relative dielectric constant was calibrated to be 8.0. Then the front and back sides were metallized with 200-nm-thick Au as the contact electrodes. $C-V$ measurements were conducted with a frequency of 100 kHz at 77 K. Subsequently the MOS capacitors were loaded into the SQUID magnetometer to record bias-dependent magnetization measurements at different temperatures.

It is noted that the quality of the dielectric layer is very crucial to minimize the leakage current. A relatively thick Al_2O_3 layer of 40 nm ensures a relatively small leakage current below 10^{-6} A cm^{-2}. When the leakage current exceeds 10^{-4} A cm^{-2}, the mobile carriers in the MOS capacitor leak out (Supplementary Fig. S3), leading to ineffective hole-mediation. From the $C-V$ measurements and the device simulations, it is clear that MOS capacitors with a leakage current of $<10^{-6}$ A cm^{-2} can operate from the accumulation to the inversion mode, which means that the hole concentrations can be modulated through gate bias.

References

1. Nikonov, D. & Bourianoff, G. Operation and modeling of semiconductor spintronics computing devices. *J. Supercond. Novel Magn.* **21,** 479–493 (2008).
2. Wolf, S. A. *et al.* Spintronics: A spin-based electronics vision for the future. *Science* **294,** 1488–1495 (2001).
3. Jungwirth, T., Sinova, J., Masek, J., Kucera, J. & MacDonald, A. H. Theory of ferromagnetic (III, Mn)V semiconductors. *Rev. Mod. Phys.* **78,** 809–864 (2006).
4. Dietl, T., Ohno, H., Matsukura, F., Cibert, J. & Ferrand, D. Zener model description of ferromagnetism in zinc-blende magnetic semiconductors. *Science* **287,** 1019–1022 (2000).
5. Akai, H. Ferromagnetism and its stability in the diluted magnetic semiconductor (In, Mn)As. *Phys. Rev. Lett.* **81,** 3002–3005 (1998).
6. Matsukura, F., Ohno, H., Shen, A. & Sugawara, Y. Transport properties and origin of ferromagnetism in (Ga, Mn)As. *Phys. Rev. B* **57,** R2037–R2040 (1998).
7. Yagi, M., Noba, K.-i. & Kayanuma, Y. Self-consistent theory for ferromagnetism induced by photo-excited carriers. *J. Lumin.* **94–95,** 523–527 (2001).
8. Sato, K. & Katayama-Yoshida, H. First principles materials design for semiconductor spintronics. *Semicond. Sci. Technol.* **17,** 367–376 (2002).

9. Ohno, H. *et al.* Electric-field control of ferromagnetism. *Nature* **408,** 944–946 (2000).
10. Chiba, D., Matsukura, F. & Ohno, H. Electric-field control of ferromagnetism in (Ga, Mn)As. *Appl. Phys. Lett.* **89,** 162505 (2006).
11. Myers, R. C. *et al.* Antisite effect on hole-mediated ferromagnetism in (Ga, Mn)As. *Phys. Rev. B* **74,** 155203 (2006).
12. Nazmul, A. M., Kobayashi, S. & Tanaka, S. S. M. Electrical and optical control of ferromagnetism in III–V semiconductor heterostructures at high temperature (∼100 K). *Jpn. J. Appl. Phys.* **43,** L233–L236 (2004).
13. Nepal, N. *et al.* Electric field control of room temperature ferromagnetism in III-N dilute magnetic semiconductor films. *Appl. Phys. Lett.* **94,** 132505 (2009).
14. Weisheit, M. *et al.* Electric field-induced modification of magnetism in thin-film ferromagnets. *Science* **315,** 349–351 (2007).
15. Bolduc, M. *et al.* Above room temperature ferromagnetism in Mn-ion implanted Si. *Phys. Rev. B* **71,** 033302 (2005).
16. Park, Y. D. *et al.* A group-IV ferromagnetic semiconductor: Mn_xGe_{1-x}. *Science* **295,** 651–654 (2002).
17. Pinto, N. *et al.* Magnetic and electronic transport percolation in epitaxial $Ge_{1-x}Mn_x$ films. *Phys. Rev. B* **72,** 165203 (2005).
18. Wang, Y. *et al.* Direct structural evidences of $Mn_{11}Ge_8$ and Mn_5Ge_2 clusters in $Ge_{0.96}Mn_{0.04}$ thin films. *Appl. Phys. Lett.* **92,** 101913 (2008).
19. Li, A. P. *et al.* Magnetism in Mn_xGe_{1-x} semiconductors mediated by impurity band carriers. *Phys. Rev. B* **72,** 195205 (2005).
20. Knobel, R., Samarth, N., Crooker, S. A. & Awschalom, D. D. Spin-polarized quantum transport and magnetic field-dependent carrier density in magnetic two-dimensional electron gases. *Phys. E: Low-dimens. Syst. Nanostruct.* **6,** 786–789 (2000).
21. Chen, J., Wang, K. L. & Galatsis, K. Electrical field control magnetic phase transition in nanostructured Mn_xGe_{1-x}. *Appl. Phys. Lett.* **90,** 012501 (2007).
22. Jeon, H. C. *et al.* $(In_{1-x}Mn_x)$As diluted magnetic semiconductor QDs with above room temperature ferromagnetic transition. *Adv. Mater.* **14,** 1725–1728 (2002).
23. Chen, Y. F. *et al.* Growth and magnetic properties of self-assembled (In, Mn)As QDs. *J. Vac. Sci. Technol. B* **23,** 1376–1378 (2005).
24. Holub, M. *et al.* Mn-doped InAs self-organized diluted magnetic quantum-dot layers with Curie temperatures above 300 K. *Appl. Phys. Lett.* **85,** 973–975 (2004).
25. Zheng, Y. H. *et al.* Cr-doped InAs self-organized diluted magnetic QDs with room-temperature ferromagnetism. *Chin. Phys. Lett.* **24,** 2118–2121 (2007).
26. Stroppa, A., Picozzi, S., Continenza, A. & Freeman, A. J. Electronic structure and ferromagnetism of Mn-doped group-IV semiconductors. *Phys. Rev. B* **68,** 155203 (2003).
27. Schulthess, T. C. & Butler, W. H. Electronic structure and magnetic interactions in Mn doped semiconductors. *J. Appl. Phys.* **89,** 7021–7023 (2001).
28. Schilfgaarde, M. v. & Mryasov, O. N. Anomalous exchange interactions in III–V dilute magnetic semiconductors. *Phys. Rev. B* **63,** 233205 (2001).
29. Ohno, H. Making nonmagnetic semiconductors ferromagnetic. *Science* **281,** 951–956 (1998).
30. Kulkarni, J. S. *et al.* Structural and magnetic characterization of $Ge_{0.99}Mn_{0.01}$ nanowire arrays. *Chem. Mater.* **17,** 3615–3619 (2005).
31. van der Meulen, M. I. *et al.* Single crystalline $Ge_{1-x}Mn_x$ nanowires as building blocks for nanoelectronics. *Nano Lett.* **9,** 50–56 (2008).
32. Wang, M. *et al.* Achieving high Curie temperature in (Ga, Mn)As. *Appl. Phys. Lett.* **93,** 132103 (2008).
33. Cho, Y. J. *et al.* Ferromagnetic $Ge_{1-x}M_x$ ($M = Mn, Fe,$ and Co) nanowires. *Chem. Mater.* **20,** 4694–4702 (2008).
34. Dietl, T., Ohno, H. & Matsukura, F. Hole-mediated ferromagnetism in tetrahedrally coordinated semiconductors. *Phys. Rev. B* **63,** 195205 (2001).
35. Kazakova, O., Kulkarni, J. S., Holmes, J. D. & Demokritov, S. O. Room-temperature ferromagnetism in $Ge_{1-x}Mn_x$ nanowires. *Phys. Rev. B* **72,** 094415 (2005).
36. Liu, C., Yun, F. & Morkoç, H. Ferromagnetism of ZnO and GaN: A review. *J. Mater. Sci.: Mater. Electron.* **16,** 555–597 (2005).
37. Sze, S. *Physics of Semiconductor Devices* 2nd edn (Wiley, 1981).
38. Ovchinnikov, I. V. & Wang, K. L. Voltage sensitivity of Curie temperature in ultrathin metallic films. *Phys. Rev. B* **80,** 012405 (2009).
39. Maekawa, S. *Concepts in Spin Electronics* (Oxford Univ. Press, 2006).
40. Dietl, T. & Spalek, J. Effect of thermodynamic fluctuations of magnetization on the bound magnetic polaron in dilute magnetic semiconductors. *Phys. Rev. B* **28,** 1548–1563 (1983).
41. Kitchen, D. *et al.* Hole-mediated interactions of Mn acceptors on GaAs (110) (invited). *J. Appl. Phys.* **101,** 09G515 (2007).
42. Lim, S. W., Jeong, M. C., Ham, M. H. & Myoung, J. M. Hole-mediated ferromagnetic properties in $Zn_{1-x}Mn_x$O thin films. *Jpn. J. Appl. Phys. 2* **43,** L280–L283 (2004).
43. Lyu, P. & Moon, K. Ferromagnetism in diluted magnetic semiconductor quantum dot arrays embedded in semiconductors. *Eur. Phys. J. B* **36,** 593–598 (2003).
44. Wang, K. L., Thomas, S. G. & Tanner, M. O. SiGe band engineering for MOS, CMOS and quantum effect devices. *J. Mater. Sci.: Mater. Electron.* **6,** 311–324 (1995).
45. Wojtowicz, T. *et al.* Enhancement of Curie temperature in $Ga_{1-x}Mn_xAs/Ga_{1-y}Al_yAs$ ferromagnetic heterostructures by Be modulation doping. *Appl. Phys. Lett.* **83,** 4220–4222 (2003).
46. Kuroda, S. *et al.* Origin and control of high-temperature ferromagnetism in semiconductors. *Nature Mater.* **6,** 440–446 (2007).
47. Karczewski, G. *et al.* Ferromagnetism in (Zn, Cr)Se layers grown by molecular beam epitaxy. *J. Supercond.* **16,** 55–58 (2003).
48. Jamet, M. *et al.* High-Curie-temperature ferromagnetism in self-organized $Ge_{1-x}Mn_x$ nanocolumns. *Nature Mater.* **5,** 653–659 (2006).
49. MEDICI Two-Dimensional Semiconductor Device Simulation edited by Inc. Technology Modeling Associates, Palo Alto (2005).
50. Arrott, A. Criterion for ferromagnetism from observations of magnetic isotherms. *Phys. Rev.* **108,** 1394–1396 (1957).

Acknowledgements

Author contributions

F.X., A.P.J. and K.L.W. conceived and designed the experiments. F.X., Y.W., J.K., A.H. and J.T. carried out the experiments. F.X., Y.W., J.Z., and K.L.W. wrote the manuscript with partial contribution from A.P.J. and J.K. All authors discussed the results and commented on the manuscript. F.X. and Y.W. contributed equally to this research.

Additional information

The authors declare no competing financial interests. Supplementary information accompanies this paper on www.nature.com/naturematerials. Reprints and permissions information is available online at http://npg.nature.com/reprintsandpermissions. Correspondence and requests for materials should be addressed to K.L.W.